Special Collection

Reduced-Graphene-Oxide-Based Needle-Type Field-Effect Transistor for Dopamine Sensing

Thomas Quast,[a] Federica Mariani,[b] Erika Scavetta,[b] Wolfgang Schuhmann,*[a] and Corina Andronescu*[c]

Owing to their intrinsic amplifying effect together with their temporal resolution, field-effect transistors (FETs) are gaining momentum for the detection of different biomolecules at ultra-low concentration levels such as, for example, neurotransmitters, particularly if the concentration level of the analyte is below the detection limit of commonly used electrochemical sensing methods. We demonstrate the fabrication of a spear-head reduced graphene oxide (rGO)-based FET. The fabrication of the rGO-based FET by means of an electrochemical pulse deposition technique enables a controllable process including both the deposition and reduction of the deposited graphene oxide between two carbon nanoelectrodes to form the channel of the rGO-based FET. While using double-barrel carbon nano-electrodes, the as-produced FETs offer new possibilities in terms of their applicability in very small volumes as well as the option of being positioned close to the desired measurement region. The fabrication process was evaluated and optimized to obtain rGO-based FETs with high performance. The as-fabricated devices were evaluated in terms of sensitivity and selectivity towards dopamine. The tested devices not only showed high sensitivity towards dopamine with a linear response ranging from 1 nM to 1 μM, but also maintained a similar sensing performance in the presence of 500 μM ascorbic acid.

1. Introduction

Since the discovery of its remarkable physicochemical properties, graphene strongly impacted many areas of science and technology. The ambipolar field effect[1] makes graphene particularly suitable as a channel material for the use in field effect transistor (FET) technology, thus attracting great interest in recent years. In contrast to Si-based FETs, graphene-based FETs are considered biocompatible and chemically stable.[2,3] Therefore, graphene and related materials-based devices have successfully entered the field of biosensors and bioelectronics. The first graphene-based FET was proposed by Ang et al.[4] Since that time, several studies have used graphene-based FETs in the field of biosensing, e.g. for the detection of DNA,[5] RNA,[6] glucose,[7–9] dopamine (DA)[10] and glutamate.[11]

Major drawbacks of these devices are the still high cost and low yield fabrication of single layer graphene, which is essential for graphene-based devices. Therefore, research efforts have been devoted to substitute single layer graphene by less costly materials which show similar properties. Graphene oxide (GO), a derivative of graphene which can be easily obtained in large quantities, has the advantage of being a more water-soluble material compared with graphene but the conductivity is strongly affected by the oxidation degree. GO is obtained by the chemical oxidation of graphite followed by exfoliation.[12] By chemical, thermal or electrochemical reduction of GO, reduced graphene oxide (rGO) can be generated and this appears to be a promising alternative material to graphene[12,13] since rGO exhibits similar electronic characteristics as graphene such as e.g. ambipolar transistor characteristics, when used as channel material in a FET.[14] Moreover, due to its residual non-reduced oxy-groups, like carboxyl groups on the surface, rGO possesses functional groups available for the immobilization of e.g. biomolecules, being thus a promising material for biosensors. Up to date, rGO-based FETs have been used for the detection of e.g. metal ions,[15] gases,[16] DA,[17] DNA,[18] and signals of living cells.[17] Due to the presence of functional groups on the GO surface dispersion of single-layer GO sheets in solution is possible, however, the challenge is seen in the deposition of one single GO layer as the channel of a FET. Different approaches are reported to obtain a single layer GO film, e.g. the Langmuir-Blodgett method[19] or the micro-molding in capillary method.[17] These methods require a chip-based design in order to generate the single GO layer film. Due to the rigid structure of the device as well as its micrometric dimensions, chip-based FETs can be successfully used to detect analytes in big volumes, ex-situ, but cannot be used to determine analytes in small volumes or be precisely positioned, for example in close proximity or inside a single cell.

[a] T. Quast, Prof. Dr. W. Schuhmann
Analytical Chemistry-Center for Electrochemical Sciences (CES)
Faculty for Chemistry and Biochemistry
Ruhr University Bochum, 44780 Bochum, Germany
E-mail: wolfgang.schuhmann@rub.de
[b] F. Mariani, Prof. Dr. E. Scavetta
Dipartimento di Chimica Industriale "Toso Montanari", Università di Bologna
Viale del Risorgimento 4, 40136 Bologna, Italy
[c] Prof. Dr. C. Andronescu
Chemical Technology III, Faculty of Chemistry and CENIDE – Center for Nanointegration
University Duisburg-Essen, Carl-Benz-Str. 199, 47057 Duisburg, Germany
E-mail: corina.andronescu@uni-due.de

Special Collection An invited contribution to a Special Collection on Electrochemical Sensing

Therefore, the design of novel device architectures is crucial to foresee real-time and in vivo applications of FET sensors. Recently, we proposed a needle-type FET device architecture in which channel sizes down to 200 nm could be generated. Such devices can be approached in close proximity to e.g. living cells or even penetrate the cell membrane to perform measurements inside a single cell. Hence, fabrication of a needle-type FET sensor with the detection taking place at the channel is seen as an important feature for analyte detection in confined volumes including single cells.[20,21] Beside the clear advantage in terms of positioning and high sensitivity, the fabrication of needle type FETs is comparatively simple and uses double barrel carbon nanoelectrodes (dbCNEs) as the source and drain electrodes, on which a polypyrrole film was electrochemically deposited to generate the channel of the FET. Here, rGO was used as the channel material, to take advantage of the ambipolar character of rGO that can operate in a wide potential range, enabling the detection of an high number of analytes.

Interesting targets in the field of biomolecule detection are neurotransmitters. As a key role in the function of human metabolic processes, dopamine (DA) is considered to be one of the most important neurotransmitter.[22,23] Consequently, it is important to fabricate a device able to measure low concentrations of DA at the single cell level in order to obtain improved understanding at a fundamental stage. The detection of ultra-low concentrations of DA in the presence of potentially interfering compounds (e.g. ascorbic acid, AA), which are present at substantially higher concentrations, is crucial since the basal level of DA in the brain is only in the low nM range.

This work describes the design and implementation of a needle-type rGO-based solution-gated FET. The rGO channel is formed by means of electrochemical pulse deposition of GO, which is concomitantly reduced under formation of rGO. This method makes the fabrication process controllable in terms of layer thickness and it avoids the use of hazardous chemicals for the reduction step. As a proof of concept, the developed needle-type FETs was used to detect DA in the nanomolar range and its sensitivity and selectivity towards AA were assessed.

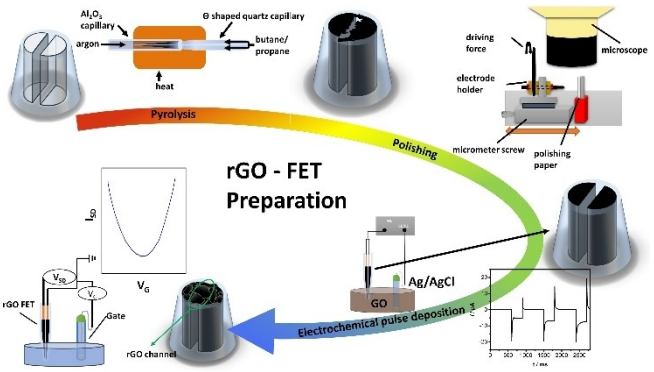

Scheme 1. Illustration of the fabrication process of a rGO-based FET.

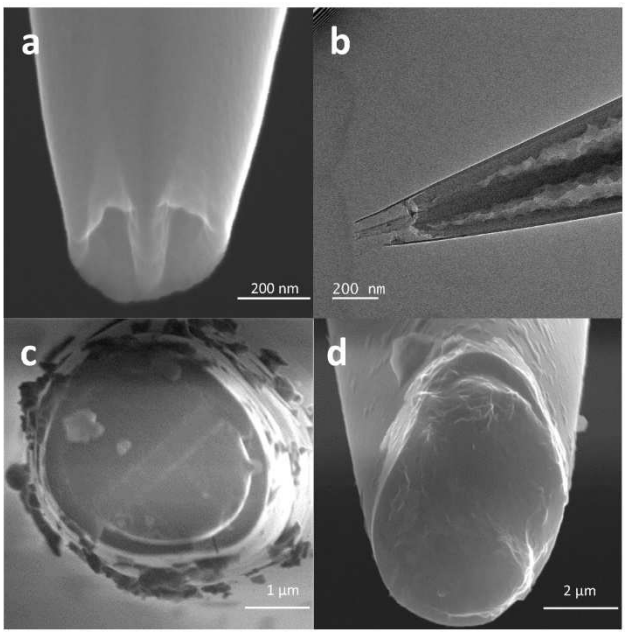

Figure 1. SEM pictures of a) a supposedly carbon-overgrown dbCNE after pyrolysis, b) a dbCNE with recessed carbon, c) a dbCNE after the polishing process, and d) a dbCNE after the electrochemical pulse deposition of GO.

2. Results and Discussion

The overall process for fabrication of needle-type rGO-based FETs is illustrated in Scheme 1.

The first step is the fabrication of double-barrel carbon nanoelectrodes (dbCNEs) using a laser-pulled theta-shaped double-barrel quartz capillary, followed by pyrolysis of a butane/propane gas mixture in an argon counter flow. Formation of dbCNEs is possible using a recently described automated pyrolysis setup.[24] However, dbCNEs often exhibit an overgrown carbon film short-circuiting both carbon nanoelectrodes (Figure 1a) or slightly recessed carbon (Figure 1b).

For the fabrication of the envisaged rGO-based FET two independent carbon nanoelectrodes separated by a thin glass wall with a well-defined planar surface are necessary. Hence, a polishing setup was developed in which the fabricated dbCNE can be precisely polished under microscope control (Scheme 1). After polishing, two independent electrodes separated by a thin glass wall were obtained (Figure 1c), however, at the expense of an increased diameter to several µm. The rGO channel of the FET is formed by electrochemical pulse deposition of GO from a homogeneous GO dispersion in water.[25,26,27] Concomitantly with the deposition of the GO flakes on the surfaces of both carbon electrodes and eventually bridging the glass wall between them, GO is electrochemically reduced under the formation of rGO (Figure 1d).

This reduction process is necessary to obtain a suitable low channel conductivity and the ability to dope the channel with the target analyte molecules. However, complete reduction to fully reduced GO is unlikely. We have used an electrochemical pulse deposition method which is indispensable to precisely control the amount of deposited GO. Different numbers of deposition pulses were applied to evaluate the optimal

parameters for the fabrication of rGO-FETs. The pulse duration was 300 ms and the reductive pulse potential was set to −1.2 V. Between each reduction pulse, the potential was kept at +0.1 V for 600 ms. 1, 3, 6, and 9 pulses were applied to dbCNEs in a two electrode setup using a Ag/AgCl/3 M KCl electrode as a quasi-reference/counter electrode.

The rGO-FETs were characterized in 0.1 M phosphate buffer solution using a Ag/AgCl/3 M KCl reference electrode as gate electrode in the configuration as shown in Scheme 1. Transfer curves were obtained by applying a fixed voltage of 50 mV between the source and drain electrode (V_{SD}) and the current flowing through the rGO channel (I_{SD}) was recorded, whereas the gate voltage (V_G) was linearly scanned with a scan rate of 100 mV s^{-1} in a potential range from 200 to 650 mV. The resulting transfer curves, as shown in Figure 2a, demonstrate the strong ambipolar field effect of the rGO-FET leading to the typical V shape due to the electronic conduction for rGO relying on both charge carriers, i.e. either holes or electrons, depending on the applied gate voltage. The lowest I_{SD} is obtained at the so-called Dirac point at which no majority charge carriers exist. Moreover, Figure 2 also displays the impact of the different number of deposition pulses on the FET performance. A functioning device can already be achieved upon application of one reductive GO deposition pulse. However, applying 3 deposition pulses clearly improved the response, leading to the highest channel conductivity. Further increase of the number of applied pulses led to a decay in the performance, most likely due to the inherently high conductivity of the channel with the higher number of rGO layers deposited at a higher number of pulses. This is in accordance with previous findings by He et al.,[17] who demonstrated that with an increasing amount of deposited rGO the field effect was decaying. Figure 2b reports the transconductance (g_m) plots obtained from the transfer curves. g_m is the parameter which describes how much the source-drain current varies by modulating the hole or electron concentration in the channel of the rGO-FET upon gate action.

The rGO-FETs were investigated with respect to their ability to detect dopamine (DA) with high sensitivity and selectivity. The proposed sensing mechanism and the measurement setup are illustrated in Figure 3. At the chosen pH value of 7.4 of the phosphate buffer solution, DA is positively charged. Due to its aromatic character, DA can interact with the electron-rich π-system of the rGO channel by means π-π stacking. The adsorbed positively charged DA molecules induce a doping of the channel by increasing the hole concentration[28] which in turn leads to a shift of the Dirac point to a more positive gate voltage and an increase in the channel conductivity. For the evaluation of the fabricated rGO-FETs with respect to their sensitivity towards DA detection, transfer curves in the absence and presence of DA in 0.1 M phosphate buffer solution were recorded. After each addition of DA, a transfer curve was recorded (Figure 4a). The rGO-FET showed the expected shift of the Dirac point to more positive gate voltages with increasing DA concentration. Simultaneously, the conductance of the channel increased significantly. Most importantly, DA concentrations as low as 1 nM could be clearly distinguished and a linear relation between source-drain current variations and the

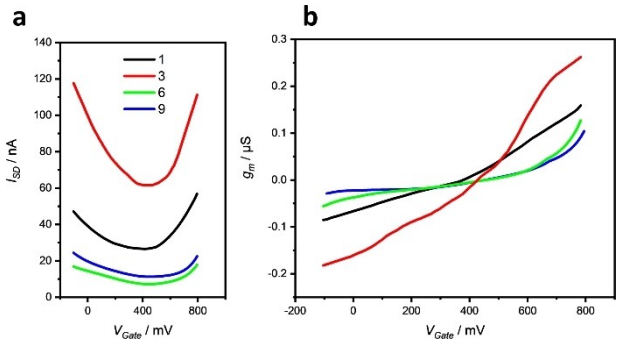

Figure 2. a) Transfer curves of rGO-FETs fabricated with different numbers of deposition pulses: 1 (black), 3 (red), 6 (green), and 9 (blue). V_{SD} = 50 mV, scan rate for V_G = 100 mV s^{-1}. b) Transconductance (g_m) plots derived from (a).

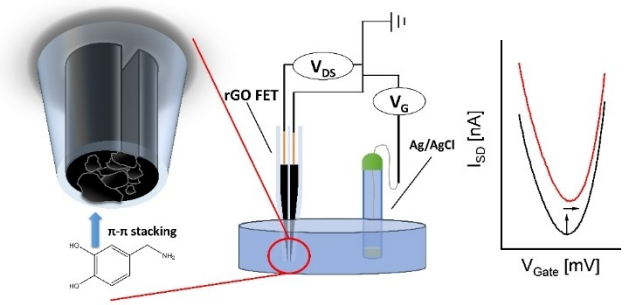

Figure 3. Electrode configuration of the measurement setup and illustration of the shift in the transfer curve of the rGO-FET upon addition of 100 µM DA (red curve).

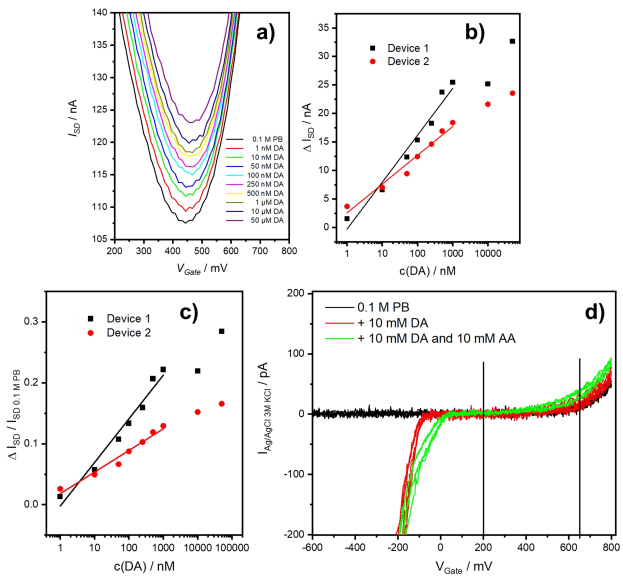

Figure 4. a) Transfer curves recorded in 0.1 M PB pH 7.4 with increasing DA concentrations from 0 to 50 µM. V_{SD} = 50 mV; scan rate 100 mV s^{-1}. b) Calibration curve obtained from two independent devices at V_G = +200 mV. c) Calibration curves normalized to I_{SD} in absence of DA. d) Cyclic voltammogram using the gate electrode as working electrode and the FET channel as counter electrode in a potential range from 800 to −600 mV at a scan rate of 100 mV s^{-1} in absence and presence of DA and AA.

logarithm of DA concentration was obtained in the range from 1 nM to 1 μM DA. Moreover, due to the individual fabrication process on the nanoscale, the double-barrel electrodes used for FET fabrication were evaluated using SEM and the overall area was determined to be $909 \pm 307\ nm^2$ ($n = 30$). Evidently, the channel dimensions and the exposed DA adsorption area cannot be more reproducible than the initial deviation of the nanosensor size. Both calibration graphs have a regression coefficient of $R^2 = 0.971$ and 0.967, respectively, and a sensitivity for DA of 8.22 ± 0.63 and 5.04 ± 0.41 nA/dec, respectively. The linear correlation between the logarithm of the DA concentration and the source-drain current is only a simplified approach to demonstrate low detection limit, high sensitivity and a wide correlation range. However, for the modulation of the source-drain current the impact of DA on the channel conductivity is essential which is governed among others by the thickness of the rGO layer, the modulation of the electron density by DA adsorption. Since the convolution of all these influences on the charge carrier mobility is evidently not to be expressed by a simple mathematical relation we were approximating the change of source-drain current with the DA concentration by a linear fit.

In order to represent the individual properties of each device, the calibration curve was also normalized by the initial I_{SD} in absence of DA (Figure 4c). Both calibration graphs have a regression coefficient of $R^2 = 0.971$ and 0.967, respectively, and a sensitivity for DA of 0.0716 ± 0.0056 and 0.0355 ± 0.0029 a.u. decade^{-1}, respectively.

In order to exclude that after adsorption of DA the rGO of the channel is further reduced under concomitant DA oxidation leading to the observed change in the transfer curve, we performed cyclic voltammograms at the gate electrode used as working electrode in an extended potential range from 800 to −600 mV at a scan rate of 100 mV s^{-1} (Figure 4d). Typically, for recording the transfer curves a potentiodynamic experiment was performed at a scan rate of 100 mV/s in a potential range between 200 and 650 mV applied to the gate electrodes. The channel is hence the polarized to potentials of opposite sign and oxidation of DA or DA/AA is expected at lower gate voltages. The voltammograms shown in Figure 4d clearly demonstrate that DA oxidation only starts at gate potentials of below −100 mV and AA oxidation occurs at gate potentials below 0 mV, both values being far more negative than the potential range chosen for recording the FET transfer curves. Hence, further reduction of the reduced graphene oxide due to dopamine oxidation can be excluded. Moreover, a significant electrochemical reduction of the rGO does not occur in the chosen potential range. We attempted to investigate the rGO layer by means of SEM before and after recording transfer curves for a prolonged time, however, due to the very thin film of deposited rGO the observed changes do not allow conclusions about the channel stability. We performed a long-term measurement at a fixed applied gate voltage and in presence of DA without significant changes in the measure I_{SD} (data mot shown).

The concentration of ascorbic acid (AA) in the brain is known to range between 200–500 μM depending on the brain region.[29] The concentration of AA is rather constant and significantly higher than the concentration of DA, typically exhibiting a basal level in the low nM region.[30] Hence, it is important to evaluate the selectivity of any highly sensitive DA sensor with respect to its co-sensitivity to AA in concentrations exceeding those of DA by at least a factor of 10^3 to 10^4. Most importantly, in the anticipated in-vivo measurements the AA concentration contributes to a constant background I_{SD}. In order to evaluate the cross-selectivity of DA and AA, an increasing concentration of AA was added to the test solution and transfer curves were recorded (Figure 5). The addition of AA caused a significant change in I_{SD} of the rGO-FET.[31] AA induces n-doping but due to the lack of a π-system capacitive-coupled interactions with the rGO channel is prevented. Hence, the change in the charge carrier concentration is substantially smaller than in the case of DA. However, even at the final concentration of AA of 500 μM, the rGO-FET was highly sensitive to subsequent additions of DA. Also, in this case, I_{SD} was changing significantly upon addition of only 1 nM DA. The change in the I_{SD} was scaling linearly with the logarithm of the DA concentration. The rGO-FET used for the measurements shown in Figure 5 was subsequently used for chronoamperometric tests. V_{SD} was set to 50 mV and the applied V_G was fixed at +600 mV, hence, the rGO-FET was operated in the n-type region. Since DA is a p-type dopant and is thus increasing the hole concentration in the channel, it is expected that I_{SD} decreases upon addition of DA (Figure 6a).

As a possibly interfering molecule, AA was added to the solution previous to DA additions and only a tiny change in I_{SD} was recorded. Upon addition of 10 nM DA I_{SD} was changing significantly with a fast response time of only 2.60 ± 0.19 s Moreover, also for the chronoamperometric measurement a linear relation of I_{SD} and the logarithm of the DA concentration was observed.

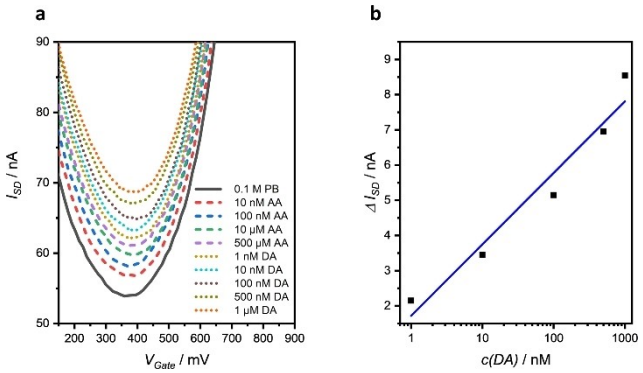

Figure 5. a) Transfer curves recorded in 0.1 m phosphate buffer, pH 7.4 upon additions of 10 nM to 500 μM AA (dashed lines) followed by additions of 1 nM to 1 μM DA (dotted lines). $V_{SD} = 50$ mV, scan rate = 100 mV s^{-1}. b) Calibration curve derived from a) showing ΔI_{SD} at $V_G = +200$ mV vs the DA concentration ($R^2 = 0.951$ with a sensitivity of 2.03 ± 0.26 nA/dec).

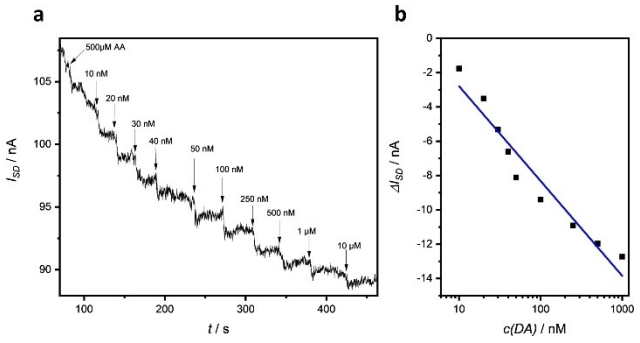

Figure 6. a) Chronoamperometric measurement of I_{SD} at $V_G = +600$ mV and $V_{SD} = +50$ mV upon initial addition of AA followed by the addition of increasing concentrations of DA b) Calibration curve for DA obtained from a) showing the ΔI_{SD} as a function of the DA concentration ($R^2 = 0949$ with a sensitivity of -5.52 ± 0.53 nA/dec).

3. Conclusions

A new needle-type rGO-based FET with dimensions in the low µM range is proposed for the highly sensitive and selective detection of dopamine. The rGO-FET was obtained by electrochemical pulse deposition of GO on a double-barrel carbon nanoelectrode separated by a thin glass wall. The proposed pulse deposition made the fabrication of the rGO-FETs controllable since not only the amount of deposited GO, but also the degree of simultaneous reduction of GO to rGO was determined by the chosen pulse profile. As a proof of concept, the obtained rGO-FETs were evaluated with respect to their ability of highly sensitive DA detection (about 5 nA/dec despite the very small FET dimensions, and ultra-low concentrations of DA (1 nM) with a fast response time of 2.60 ± 0.19 s were successfully developed. Thanks to the size and shape of the FET sensor, measurements at single living cells during stimulated DA exocytosis should be feasible in the future, especially due to the fact that the basal DA level can be detected even in the presence of high concentrations of AA. Major limitations are the uniqueness of each FET and the limited long-term stability, issues which are presently under investigation.

Experimental Section

Preparation of rGO-FETs. Double-barrel theta-shaped quartz capillaries (outer diameter 1.2 mm, inner diameter 0.9 mm, Sutter Instruments) were pulled using a Laser puller P-2000 (Sutter Instruments) with the following parameters: Heat = 780, Filament = 4, Velocity = 45, Delay = 130, Pull = 90. The pulled capillaries were filled with carbon by pyrolysis of a butane/propane gas mixture (Air Liquide). Afterwards, the generated electrodes were polished under microscope control using a specifically developed polishing setup on aluminum oxide grinding paper with a grain size of 0.3 µM (3 M). For electrical connection, copper wires were inserted into the prepared dbCNEs. The needle-type rGO-FETs were obtained by formation of a channel upon connection of the individual carbon electrodes by the electrodeposited rGO. For this, a suspension of 2 mg ml^{-1} GO in water (Sigma Aldrich) was diluted to 0.5 mg ml^{-1} and sonicated for 2 h before use. Pulse deposition at the dbCNEs was performed using a VA-10 voltammetric amplifier (npi electronic) in a two electrode configuration with a Ag/AgCl/3 M KCl quasi-reference/counter electrode. A reductive pulse potential of −1.2 V vs. Ag/AgCl/3 M KCl was applied for 300 ms. In between reductive pulses the potential was kept at +0.1 V vs Ag/AgCl/3 M KCl for 600 ms. During the pulse deposition the two electrodes of the dbCNEs were shortcut by two connected copper wires.

Electrochemical characterization. The rGO-FETs were characterized inside a Faraday cage using two VA-10 voltammetric amplifiers (npi electronic). The grounds of both devices were coupled and connected to the source electrode. The working electrode of one amplifier was used as the drain while the working electrode of the second amplifier was used as the gate. The rGO-FETs were characterized using 0.1 M phosphate buffer, pH 7.4, as electrolyte solution prepared from Na_2HPO_4 (VWR) and NaH_2PO_4 (J.T. Baker). A dopamine stock solution with a concentration of 0.1 M DA was prepared using the same phosphate buffer solution. Therefore, the stock solution was diluted to different concentration levels (10^{-3}, 10^{-4}, and 10^{-5} M DA) for calibration measurements. Ascorbic acid (Sigma Aldrich) solutions were prepared likewise. All chemicals were used as received and water was deionized using a water purification system (SG). The source-drain current (I_{SD}) was continuously monitored while a constant voltage between the source and drain electrode (V_{SD}) of 50 mV was applied before different concentrations of DA or AA were added. After each addition, the solution was stirred by using a second pipette tip. The gate voltage was kept at constant voltage (+600 mV) for chronoamperometric measurements or was modulated by applying a voltage ramp at a scan rate of 100 mV s^{-1}, as indicated.

Acknowledgements

This work was financially supported by the Deutsche Forschungsgemeinschaft (DFG, German Research Foundation) in the framework of the project FLAG-ERA JTC 15 "Graphtivity" (Schu929/14-1).

Conflict of Interest

The authors declare no conflict of interest.

Keywords: spearhead field-effect transistors · graphene oxide · dopamine · bioelectronics · neurotransmitter

[1] K. S. Novoselov, A. K. Geim, S. V. Morozov, D. Jiang, Y. Zhang, S. V. Dubonos, I. V. Grigorieva, A. A. Firsov, *Science* **2004**, *306*,666–669.
[2] Y. Liu, D. Yu, C. Zeng, Z. Miao, L. Dai, *Langmuir* **2010**, *26*, 6158–6160.
[3] C. Liao, Y. Li, S. C. Tjong, *Int. J. Mol. Sci.* **2018**, *19*, 3564.
[4] P. K. Ang, W. Chen, A. T. S. Wee, K. P. Loh, *J. Am. Chem. Soc.* **2008**, *130*, 14392–14393.
[5] T.-Y. Chen, P. T. K. Loan, C.-L. Hsu, Y.-H. Lee, J. T.-W. Wang, K.-H. Wei, C.-T. Lin, L.-J. Li, *Biosens. Bioelectron.* **2013**, *41*, 103–109.
[6] B. Cai, L. Huang, H. Zhang, Z. Sun, Z. Zhang, G.-J. Zhang, *Biosens. Bioelectron.* **2015**, *74*, 329–334.
[7] M. Zhang, C. Liao, C. H. Mak, P. You, C. L. Mak, F. Yan, *Sci. Rep.* **2015**, *5*, 8311.
[8] J. W. Park, C. Lee, J. Jang, *Sens. Actuators B* **2015**, *208*, 532–537.
[9] Y. H. Kwak, D. S. Choi, Y. N. Kim, H. Kim, D. H. Yoon, S. S. Ahn, J.-W. Yang, W. S. Yang, S. Seo, *Biosens. Bioelectron.* **2012**, *37*, 82–87.
[10] M. Zhang, C. Liao, Y. Yao, Z. Liu, F. Gong, F. Yan F, *Adv. Funct. Mater.* **2014**, *24*, 978–985.

[11] Y. Huang, X. Dong, Y. Shi, C. M. Li, J.-J. Li, P. Chen, *Nanoscale* **2010**, *2*, 1485–1488.
[12] S. Stankovich, D. A. Dikin, R. D. Piner, K. A. Kohlhaas, A. Kleinhammes, Y. Jia, Y. Wu, S. T. Nguyen, R. S. Ruoff, *Carbon* **2007** *45*, 1558–1565.
[13] S. Park, R. S. Ruoff, *Nanotechnology* **2009**, *4*, 217–224.
[14] G. Eda, G. Fanchini, M. Chhowalla, *Nat. Nanotechnol.* **2008**, *3*, 270–274.
[15] H. G. Sudibya, Q. He, H. Zhang, P. Chen, *ACS Nano.* **2011**, *5*, 1990–1994.
[16] K. Toda, R. Furue, S. Hayami, *Anal. Chim. Acta* **2015**, *878*, 43–53.
[17] Q. He, H. G. Sudibya, Z. Yin, S. Wu, H. Li, F. Boey, W. Huang, P. Chen, H. Zhang, *ACS Nano* **2010**, *4*, 3201–3208.
[18] Z. Yin, Q. He, X. Huang, J. Zhang, S. Wu, P. Chen, G. Lu, Q. Zhang, Q. Yan, H. Zhang, *Nanoscale* **2012**, *4*, 293–297.
[19] L. J. Cote, F. Kim, J. Huang, *J. Am. Chem. Soc.* **2009**, *131*, 1043–1049.
[20] Y. Zhang, J. Clausmeyer, B. Babakinejad, A. L. Córdoba, T. Ali, A. Shevchuk, Y. Takahashi, P. Novak, C. Edwards, M. Lab, S. Gopal, C. Chiappini, U. Anand, L. Magnani, R. C. Coombes, J. Gorelik, T. Matsue, W. Schuhmann, D. Klenerman, E. V. Sviderskaya, Y. Korchev, *ACS Nano* **2016**, *10*, 3214–3221.
[21] D. Son, S. Y. Park, B. Kim, J. T. Koh, T. H. Kim, S. An, D. Jang, G. T. Kim, W. Jhe, S. Hong, *ACS Nano* **2011**, *5*, 3888–3895.
[22] J. Meiser, D. Weindl, K. Hiller, *Cell Commun. Signaling* **2013**, *1*, 34.
[23] R. de la Fuente-Fernández, T. J. Ruth, V. Sossi, M. Schulzer, D. B. Calne, A. J. Stoessl, *Science* **2001**, *293*,1164–1166.
[24] P. Wilde, T. Quast, H. B. Aiyappa, Y.-. T. Chen, A. Botz, T. Tarnev, M. Marquitan, S. Feldhege, A. Lindner, C. Andronescu, W. Schuhmann, Y.-T. Chen, *ChemElectroChem* **2018**, *5*, 3083–3088.
[25] M. Hilder, B. Winther-Jensen, D. Li, M. Forsyth, D. R. MacFarlane, *Phys. Chem. Chem. Phys.* **2011**, *13*, 9187–9193.
[26] Y. Shao, J. Wang, M. Engelhard, C. Wang, Y. Lin, *J. Mater. Chem.* **2010**, *20*, 743–748.
[27] G. K. Ramesha, S. Sampath, *J. Phys. Chem. C* **2009**, *113*, 7985–7989.
[28] X. Dong, D. Fu, W. Fang, Y. Shi, P. Chen, L.-J. Li, *Small* **2009**, *5*, 1422–1426.
[29] R. A. Grünewald, *Brain Res. Rev.* **1993**, *18*, 123–133.
[30] B. J. Venton, H. Zhang, P. A. Garris, P. E. M. Phillips, D. Sulzer, R. M. Wightman, *Neurochem.* **2003**, *87*, 1284–1295.
[31] J. Zhang, H. Yang, G. Shen, P. Cheng, J. Zhang, S. Guo, *Chem. Commun.* **2010**, *46*, 1112–1114.

Manuscript received: January 30, 2020
Revised manuscript received: March 29, 2020
Accepted manuscript online: March 30, 2020